



## NRC Publications Archive Archives des publications du CNRC

### **The interaction field in arrays of ferromagnetic barcode nanowires** Clime, L.; Zhao, S. Y.; Chen, P.; Normandin, F.; Roberge, H.; Veres, T.

This publication could be one of several versions: author's original, accepted manuscript or the publisher's version. / La version de cette publication peut être l'une des suivantes : la version prépublication de l'auteur, la version acceptée du manuscrit ou la version de l'éditeur.

For the publisher's version, please access the DOI link below. / Pour consulter la version de l'éditeur, utilisez le lien DOI ci-dessous.

#### **Publisher's version / Version de l'éditeur:**

<https://doi.org/10.1088/0957-4484/18/43/435709>

*Nanotechnology*, 18, 43, pp. 435709-1-435709-6, 2007-10-04

#### **NRC Publications Record / Notice d'Archives des publications de CNRC:**

<https://nrc-publications.canada.ca/eng/view/object/?id=500b1f18-909f-4d34-940d-52bce2212765>

<https://publications-cnrc.canada.ca/fra/voir/objet/?id=500b1f18-909f-4d34-940d-52bce2212765>

Access and use of this website and the material on it are subject to the Terms and Conditions set forth at

<https://nrc-publications.canada.ca/eng/copyright>

READ THESE TERMS AND CONDITIONS CAREFULLY BEFORE USING THIS WEBSITE.

L'accès à ce site Web et l'utilisation de son contenu sont assujettis aux conditions présentées dans le site

<https://publications-cnrc.canada.ca/fra/droits>

LISEZ CES CONDITIONS ATTENTIVEMENT AVANT D'UTILISER CE SITE WEB.

**Questions?** Contact the NRC Publications Archive team at

PublicationsArchive-ArchivesPublications@nrc-cnrc.gc.ca. If you wish to email the authors directly, please see the first page of the publication for their contact information.

**Vous avez des questions?** Nous pouvons vous aider. Pour communiquer directement avec un auteur, consultez la première page de la revue dans laquelle son article a été publié afin de trouver ses coordonnées. Si vous n'arrivez pas à les repérer, communiquez avec nous à PublicationsArchive-ArchivesPublications@nrc-cnrc.gc.ca.



# The interaction field in arrays of ferromagnetic barcode nanowires

L Clime<sup>1</sup>, S Y Zhao<sup>1</sup>, P Chen<sup>2</sup>, F Normandin<sup>1</sup>, H Roberge<sup>1</sup> and T Veres<sup>1</sup>

<sup>1</sup> NRC, Industrial Materials Institute, 75 de Mortagne Boulevard, Boucherville, J4B 6Y4, Canada

<sup>2</sup> Research Center for Applied Sciences, Academia Sinica 128 Section 2, Academia Rd, Nankang, Taipei 11529, Taiwan

E-mail: [Liviu.Clime@nrc.ca](mailto:Liviu.Clime@nrc.ca)

Received 20 July 2007, in final form 23 August 2007

Published 4 October 2007

Online at [stacks.iop.org/Nano/18/435709](http://stacks.iop.org/Nano/18/435709)

## Abstract

A theoretical model and an experimental approach to the identification of the interaction field in ferromagnetic barcode nanowires are described and applied to electrodeposited Ni/Au cylindrical barcode arrays. Elementary hysteresis loops of individual magnetic segments in these barcode nanowires are considered as superpositions of fully irreversible and locally reversible magnetization processes, whose distributions of switching fields are experimentally identified by first order reversal curve measurements. Non-interacting major hysteresis loops of the arrays are computed as superpositions of several elementary loops by considering the distributions of switching fields as probability density functions. The interaction field is then computed from the condition that the geometric transformation of the experimental major hysteresis loop into the Preisach operative plane be well approximated by this non-interacting hysteresis loop. Experimental interaction field values are compared with those obtained by numerical micromagnetic computations and a very good agreement is obtained on extended Ni/Au barcode arrays. The simple and accurate phenomenological model for the interaction field in multisegmented ferromagnetic nanowire arrays proposed here provides an insight into the morphology of these magnetic nanomaterials, as quantitative information about individual nano-objects may be extracted from macroscopic measurements of their arrays.

(Some figures in this article are in colour only in the electronic version)

## 1. Introduction

There has been continuously increased interest in the fabrication and characterization of nanostructured ferromagnetic nanowire arrays due to their potential applications in magnetic recording media and sensors [1, 2], synthesis of carriers for magnetic manipulation in bio-medical applications [3–6], MEMS devices [7] or magnetic nano-assembly [8–10]. The advantages of these nanowires over classical superparamagnetic particles are mainly related to the possibility of favorable tailoring of their intrinsic and geometric anisotropies [2, 11–13] and to their increased magnetic moments due to the permanent saturation magnetization of ferromagnetic materials. However,

magnetic interactions in colloidal suspensions of contiguous magnetic nanowires may induce additional problems related to aggregation, and consequently strategies involving segmented (barcode) nanowires consisting of alternating magnetic and non-magnetic segments [12–15] may become suitable for accurate manipulation and positioning [10].

Among the techniques widely employed for the characterization of magnetic nanostructures, magnetometry plays an important role due to its low cost and high sensitivity. However, when intrinsic properties of individual nano-objects have to be extracted from magnetic measurements of their arrays, an important problem related to the stray (demagnetization) field in these nanostructures has to be addressed. Several nu-

merical approaches for clusters of superparamagnetic spherical particles [16], ferromagnetic objects of arbitrary shapes [17] or regular arrays of ferromagnetic nanowires [18–27] are available in the literature, but their applicability to extended arrays is limited to either a relatively small number or limited size of individual nano-objects.

In this paper we extend the phenomenological model for the interaction field in arrays of contiguous nanowires as proposed in [28, 29], to arrays of ferromagnetic segmented nanowires. Moreover, we present an experimental approach to the identification of the interaction field from major hysteresis loop (MHL) and partial first order reversal curve (FORC) measurements [30]. Comparisons between the proposed theoretical model and experimental measurements of electrodeposited Ni/Au segmented nanowire arrays with three different aspect ratios are made and a very good agreement is obtained.

The paper is organized as follows. Section 2 contains a brief description of the experimental approach employed for the synthesis of Ni–Au barcode arrays, followed by a description of the magnetic measurements used in the identification of the interaction field (section 3). Section 4 presents the proposed theoretical model for the interaction field in extended arrays of multi-segmented ferromagnetic nanowires. Experimental and theoretical values for the interaction field are compared and discussed in section 5, after which we end with some concluding remarks.

## 2. Experimental details

Anodized aluminum oxide (AAO) porous membranes prepared by a two-step anodization method developed by Masuda and Fukuda [31] (and described in [11] and [32]) have been used in order to grow magnetic nanowires via a DC electrodeposition technique [33]. A 300 nm Au film was firstly sputtered on the back side of the open through template in order to obtain a working electrode. The electrochemical plating is led into the pores of AAO membranes only by painting two layers of photoresist (S-1805) on both the sample back and edge and evaporating the solvent at 200 °C. All the electrochemical plating was done at room temperature in a classical three-electrode configuration. A saturated calomel electrode (SCE) and a Pt foil were used as reference electrode and counterelectrode, respectively. The electrolysis bath consists of  $\text{HAuCl}_4 \cdot 3\text{H}_2\text{O}$  (2 mM),  $\text{NiCl}_2 \cdot 6\text{H}_2\text{O}$  (2 M), and  $\text{H}_3\text{BO}_3 \cdot 2\text{H}_2\text{O}$  (0.5 M), whereas the current density is controlled via a PAR 273A potentiostat/galvanostat. The multilayer structure of the magnetic nanowires is then obtained by a pulsed electrodeposition technique, by periodically switching the current density between  $0.5 \text{ mA cm}^{-2}$  for Au and  $5 \text{ mA cm}^{-2}$  for Ni. Lengths of both magnetic and non-magnetic segments in individual barcodes are controlled via the electrodeposition time corresponding to the above mentioned current density values. In this way, we build arrays of almost parallel barcode nanowires consisting of alternating magnetic and non-magnetic regions, whose lengths  $x$  and  $y$  (figure 1) can easily be controlled by the electrodeposition time.

In figure 2 we present SEM lateral views of broken membranes for three arrays of electrodeposited barcodes obtained by the above mentioned procedure with non-magnetic

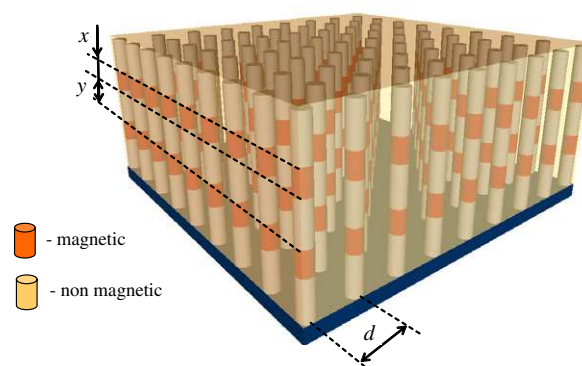


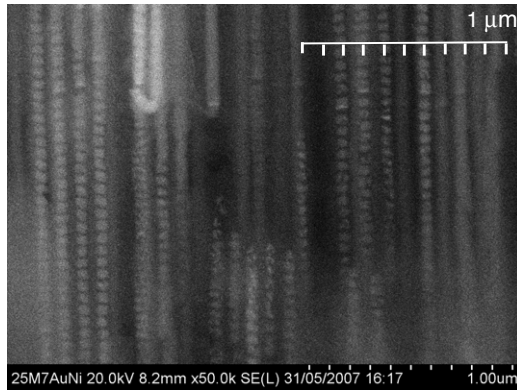
**Figure 1.** Schematic representation of a small region in a segmented ferromagnetic barcode array.

(Au) segments of about the same length (50 nm). The magnetic (Ni) inclusions present different lengths from one sample to another, namely 10 nm (a), 18 nm (b) and 30 nm (c), corresponding to electrodeposition time intervals of 1, 2 and 5 s and further referred to as samples A–C, respectively. The radius of the nanowires is about 70 nm and does not vary too much from one nanowire to another, as the electrodeposition membranes present a good monodispersity of the pore diameter [11]. The nanowires exhibit hexagonally centered symmetry [11, 32] with an average lattice constant of about 85 nm (figure 2).

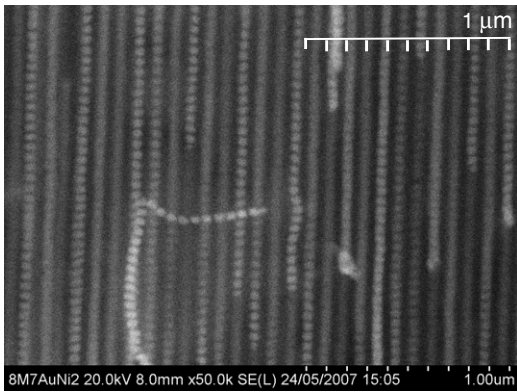
The layer thickness and the morphology of barcode nanowires were determined by scanning electron microscopy (SEM) with a Hitachi S-4800 microscope whereas DC major hysteresis loops (MHLs) and first-order reversal curves (FORCs) were measured with a Quantum Design physical property measurement system (PPMS). Different magnetic loads in individual magnetic wires influence the overall magnetic behavior of their arrays, the main effect being related to the variation of the magnetic susceptibility with respect to the magnetic to non-magnetic content ratio (the slope of the MHLs in figure 3 decreases as magnetic loads in individual nanowires get larger). As we can see in the next section, the slope of these loops, in conjunction with accurate FORC evaluations of the switching fields, can be used in order to identify the interaction field in these nanostructures.

## 3. Hysteresis loops

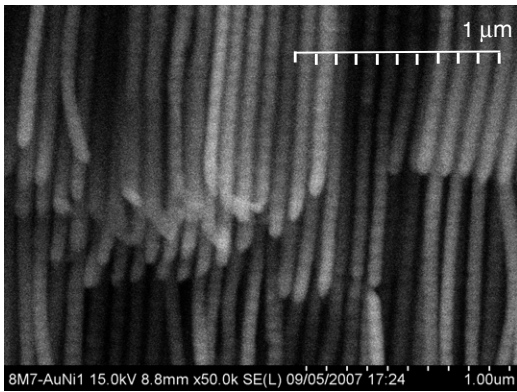
The theoretical approach employed here in order to model the hysteresis loops of arrays of ferromagnetic barcode nanowires is inspired by the Preisach-type models [34]. Firstly, non-interacting loops of these arrays are obtained by linear superpositions of magnetization processes in individual ferromagnetic segments (considered as hysterons [34]). Then, overall hysteresis loops of interacting nanowires are obtained by simple linear transformation of the non-interacting ones into the operative Preisach plane [34, 35]. This geometric transformation is performed under the assumption that the interaction field is proportional to the total magnetization of the sample [34, 36]. Therefore the identification of the interaction field in arrays of magnetic nanowires requires information about magnetization processes in individual nanowires, distributions of switching fields and overall magnetization loops of the arrays [35]. In the following,



a)



b)



c)

**Figure 2.** SEM views of Ni/Au barcode nanowire arrays for three different non-magnetic to magnetic length ratios:

(a) Au = 50 nm/Ni = 10 nm; (b) Au = 50 nm/Ni = 18 nm; (c) Au = 50 nm/Ni = 30 nm. The total length of the scale in these figures is 1  $\mu$ m.

we describe how these requirements have been addressed from a theoretical point of view, the results obtained from experimental measurements being presented in section 4.

The hysteresis loop of a single magnetic segment in a barcode nanowire is considered to be dominated by irreversible magnetization reversals that produce square loops

$$m(H) = \begin{cases} +1, & H \geq H_c \\ -1, & H < H_c, \end{cases} \quad (1)$$

with some ‘rounding’ near the transition points toward and

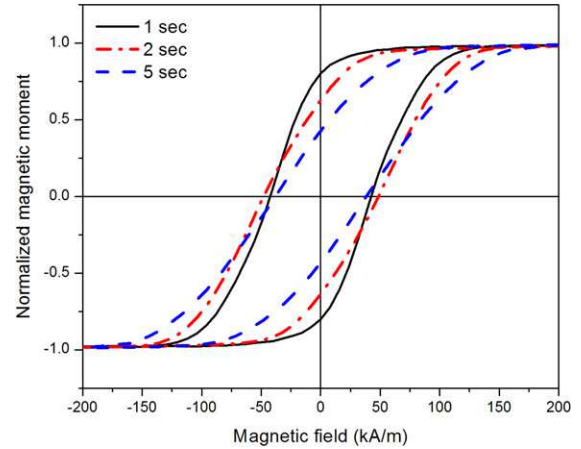


**Figure 3.** Experimental axial MHL measurements of barcode arrays with different magnetic loads corresponding to Ni electrodeposition time intervals of 1, 2 and 5 s.

from saturation [34, 35]

$$m_r(H) = \pm (1 - q) e^{\mu\zeta H}, \quad (2)$$

due to the reversible part of the magnetization processes.  $q$  and  $\zeta$  in equation (2) are two phenomenological parameters related to the ‘squareness’ of the hysteresis loop [34]. The reversible part in equation (2) influences the shape of the magnetization loops near saturation rather than the slope near the zero-magnetization states, the latter being mainly related to the strength of the interaction field. However, even if it is strictly phenomenological, that is it does not account for the real origin of the reversible processes in individual magnetic nanoparticles, a better fit of the experimental magnetization loops can be obtained if this reversibility is taken into account.

The distribution of switching fields  $\rho(H_c)$  is directly extracted from first order reversal curve measurements [30]. In this kind of measurements, the sample is initially saturated in strong magnetic field  $H_{\text{sat}}$  and the field ramped down to zero. The magnetic moment is then measured at three values of the applied field, namely 0,  $\Delta H$  and  $2\Delta H$ , after this the sample being again saturated by applying  $H_{\text{sat}}$ . Further reversal fields are chosen as negative multiples of  $\Delta H$  and the magnetic moment measured at five points centered at these reversal points and equally spaced with  $\Delta H$ . The distribution of switching fields is the second order mixed derivative of the experimental bivariate function  $m(H, H_r)$  along the diagonal points of the Preisach plane [30]

$$S(H_c) = -\frac{1}{2} \frac{\partial^2 m}{\partial H \partial H_r} \Big|_{H=-H_r}. \quad (3)$$

The experimental profiles  $S$  given by equation (3) are used as probability density functions (PDFs) in order to obtain the non-interacting MHL of the array,

$$M_{\text{NI}}(H) = \int_0^\infty S(H_c) \times m(H; H_c) dH_c. \quad (4)$$

Further on, the interacting MHL is given by the linear transformation [34, 35]

$$H_I \rightarrow H + \alpha \cdot M_{\text{NI}}, \quad (5)$$

where  $\alpha$  is a phenomenological parameter accounting for the interactions between individual magnetic nanosegments and may be considered as a good approximation for the interaction field in these nanostructures.

Since the interacting MHL is well known (from experimental measurements, figure 3), the parameter  $\alpha$  may be identified from the best fit of these experimental loops with (5). From this equation we may easily observe that  $\alpha$  is identical to the interaction field at saturation, since for  $M_{NI} = 1$  we get exactly  $\alpha = H_{I,sat} - H_{sat}$  [29].

In the following section we present a theoretical model that is able to accurately compute the interaction field in ferromagnetic barcode arrays by using a phenomenological analytical expression.

#### 4. Interaction field

The interaction field in assemblies of ferromagnetic nano-objects is an important topic in micromagnetics, several difficulties related to the magnetization dependence nonlinearities being reported in the literature [37]. Fully numerical micromagnetic approaches lead to relatively accurate results [23–25] but they are limited to a small number of nanowires. In order to account for the interaction field in extended nanowire arrays, we use a semi-analytical approach [29] in which the magnetic field from individual nanowires is obtained as a sum of two terms: the near field, from a small region containing only the nearest neighbors, numerically computed by discretizing each nanowire in small elements, and the far field, analytically computed by considering the remaining area as an equivalent thin film [29]. Therefore, since parameter  $\alpha$  in our analysis is mainly related to saturation states and, moreover, the direction of interest coincides with the symmetry axis of the nanowires (out-of-plane direction), a good approximation for the interaction field at saturation may be obtained [28] if we model the arrays in figure 2 as distributions of identical cylindrical barcode nanowires located at the nodes of an equivalent rectangular lattice (figure 1) and apply [28]

$$H_{int}(l, d) = M_s r^2 \frac{1}{1 + \xi} \left[ a(d) \cdot l + b(d) \tanh\left(\frac{l}{l_d}\right) \right] \quad (6)$$

where  $\xi$  is a geometric parameter related to the non-magnetic to magnetic content ratio ( $\xi = y/x$  with  $y$  and  $x$  the lengths of respectively non-magnetic and magnetic segments in the barcode—figure 1).  $M_s$  is the saturation magnetization,  $l$  the total length of barcodes,  $d$  the average interwire spacing (the constant of the equivalent rectangular lattice) and  $l_d$  a phenomenological parameter, usually of the order of a few hundred nanometers and related to the transition from the dipolar regime (very small lengths) to the monopolar one [29]. We consider a certain (irregular) lattice as ‘equivalent’ to a rectangular lattice if the number of nanowires per unit area is identical. In this view, an hexagonally centered lattice of constant  $d_{hc}$  will be equivalent to a rectangular lattice of constant  $d = \sqrt{\sqrt{3}/2} d_{hc}$ , that is  $0.93 d_{hc}$ . For the nanowires in figure 2,  $d_{hc} \cong 80$  nm; that is, the equivalent rectangular array is characterized by an equivalent lattice constant of about  $d = 75$  nm.  $a(d)$  and  $b(d)$  in equation (6) are two phenomenological functions of the distance  $d$  between

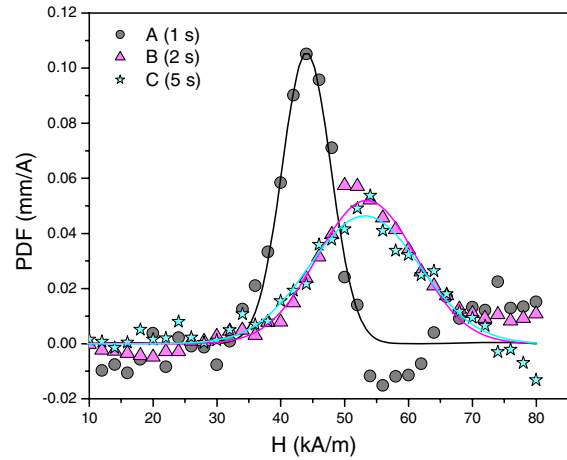


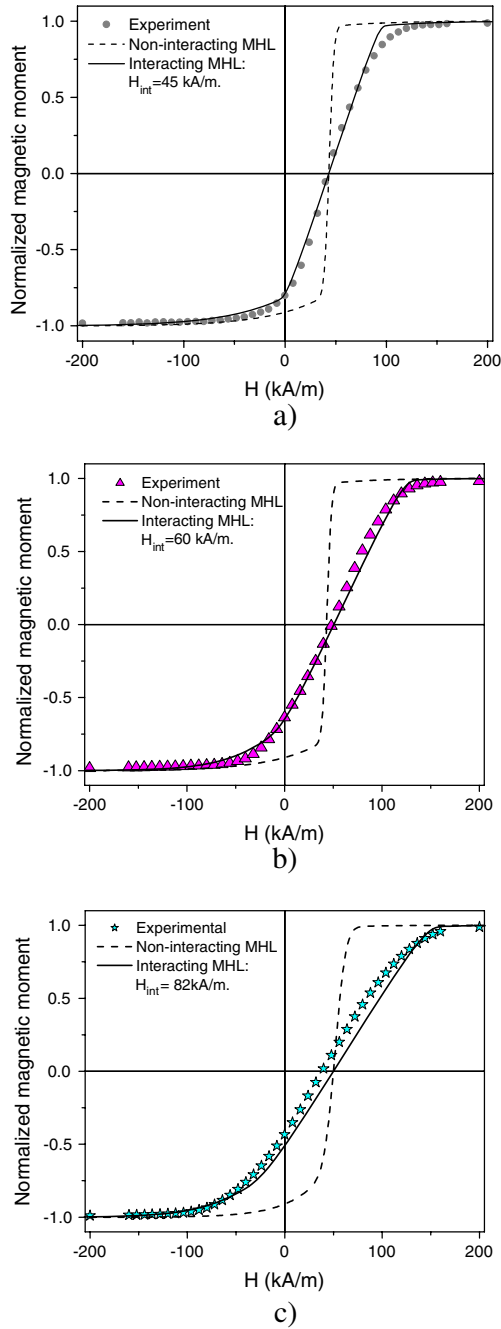
**Figure 4.** Experimental distributions of switching fields (bullets) and best fit with Gaussians (solid line).

nanowires [28]. Non-magnetic nanowires are characterized by  $\xi \rightarrow \infty$  and consequently  $H_{int} = 0$ , whereas contiguous ferromagnetic nanowires have  $\xi = 0$ .  $H_{int}$  in the latter case reduces to simpler analytical expressions, such as that given in [28], from which equation (6) is obtained by averaging the magnetization of individual barcode nanowires.

#### 5. Results and discussion

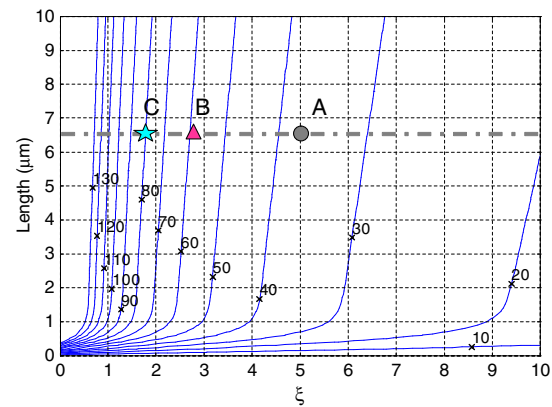
The coercive field values revealed by FORC measurements for the three samples A–C range from  $35 \text{ kA m}^{-1}$  to  $70 \text{ kA m}^{-1}$ , shorter magnetic segments being characterized by smaller values (figure 4) of this parameter. These results are in good agreement with previous micromagnetic simulations [38] and experimental measurements [39] on nickel nanowires. The experimental distributions of switching fields are interpolated with Gaussians (solid lines in figure 4) and used as probability density functions in equation (4) in order to obtain the non-interacting hysteresis loop of the array (dashed lines in figure 5). Since these non-interacting loops rely upon the experimental distribution of switching fields, it is obvious that they have to present about the same coercive field values as the experimental loading MHLs (figure 5). The difference in the magnetic susceptibility values between these two magnetization curves (experimental and non-interacting) is minimized by applying the transformation (5) to the non-interacting loops and the best value of the fitting parameter  $\alpha$  assimilated with the interaction field at saturation. The thus-obtained interacting loops are drawn with solid lines in figure 5. The legends of these graphs also contain the numerical values of the experimental interaction field obtained by the above described procedure. These values are also indicated with symbols in figures 6 and 7.

Figure 6 also gives some contour lines of the theoretical interaction field calculated with the analytical expression in equation (6) for magnetic barcode arrays whose total lengths range from a few hundred nanometers up to  $10 \mu\text{m}$  and non-magnetic to magnetic ratios  $\xi$  from 0 to 10. We considered  $d = 75$  nm for the equivalent (rectangular) lattice constant,  $r = 35$  nm for the nanowire radius and  $M_s = 0.49 \times 10^6 \text{ A m}^{-1}$  for



**Figure 5.** Experimental (symbols) and theoretical non-interacting (dashed line) and interacting (full line) loading MHLs for arrays of Au/Ni magnetic barcodes with different non-magnetic to magnetic ratios: (a)  $\xi = 5$  (A); (b)  $\xi = 2.7$  (B); (c)  $\xi = 1.6$  (C).

the saturation magnetization of the magnetic segments. For a given magnetic load  $\xi$ , the interaction field is hardly dependent on the total length of the barcodes since the contour plot lines in figure 6 are nearly vertical, especially at smaller  $\xi$ . Therefore  $H_{int}$  is not very sensitive to the total length  $l$  of the nanowires and consequently the occurrence of nanowires of different lengths in the same sample does not have to affect the accuracy of the interaction field computation. In contrast, due to the hyperbolic dependence of  $H_{int}$  on  $\xi$  (equation (6)), variations in the magnetic load at small values  $\xi$  have a huge influence on the computed interaction field (figure 7). The limit of about



**Figure 6.** Theoretical contour plot for the interaction field in barcode nanowire arrays of different lengths of magnetic load. The symbols on the diagram stand for the interaction field in extended arrays of barcodes of about the same length  $6.5 \mu\text{m}$  but different non-magnetic to magnetic ratios:  $\xi = 5$  (A),  $\xi = 2.7$  (B) and  $\xi = 1.6$  (C). Numbers on each contour line indicate the value of the interaction field in  $\text{kA m}^{-1}$ .

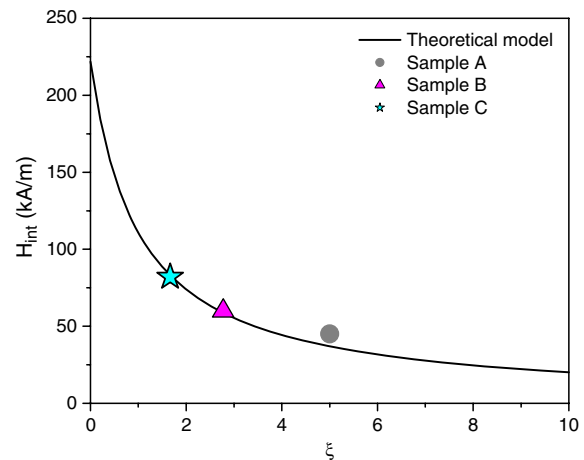


**Figure 7.** Experimental and theoretical interaction field in extended arrays of barcodes of  $6.5 \mu\text{m}$  length but different non-magnetic to magnetic ratios:  $\xi = 5$  (A),  $\xi = 2.7$  (B) and  $\xi = 1.6$  (C).

$220 \text{ kA m}^{-1}$  obtained for  $\xi = 0$  corresponds to contiguous ferromagnetic nanowires and represents the maximum value of the interaction field. Obviously, the interaction field has to vanish at  $\xi \rightarrow \infty$ , that is, when the nanowires are completely ‘non-magnetic’.

The experimental measurements and the theoretical computations of the interaction field at saturation agree very well for the arrays of ferromagnetic barcode nanowires A–C (figures 6 and 7). The non-magnetic to magnetic ratios for these samples were evaluated as  $\xi = 5$  for sample A,  $\xi = 2.7$  for sample B and  $\xi = 1.6$  for sample C. The total length of the barcode nanowires was considered to be  $6.5 \mu\text{m}$  for all three samples (dash-dotted line in figure 6) and numerical values of interaction field computed for these three different morphologies of the arrays. As we may see in figures 6 and 7, experimental values for the interaction field  $H_{int,A} = 45 \text{ kA m}^{-1}$ ,  $H_{int,B} = 60 \text{ kA m}^{-1}$  and  $H_{int,C} = 82 \text{ kA m}^{-1}$  agree very well with the theoretical model. However, a

difference of about  $6 \text{ kA m}^{-1}$  is observed for sample A (figure 7), and it may originate in the inherent imprecision in evaluating the morphology of the arrays from SEM images (figure 2(c)).

As expected, the sample containing longer magnetic segments (C) is characterized by stronger interaction fields. On MHL measurements this may be identified by lower values of the MHL slope (magnetic susceptibility). Although the strength of the interactions is related to this slope, the identification of this parameter with the interaction field at saturation is possible only for sharp distributions of the switching fields, which give rise to almost rectangular global non-interacting loops (for example sample A in figure 4 for the distribution of switching fields and figure 5 for the non-interacting MHL). Broader distributions of switching fields induce skewed non-interacting loops and the application of (4) and (5) in order to identify the strength of the interactions becomes mandatory.

The distributions of switching fields for samples B and C are very similar although the morphologies of these samples are very different (figures 2(b) and (c)). This may easily be explained by the slow dependence of the coercive field on the length of ferromagnetic nanosegments [40]. Important variations of this parameter may occur only at very small lengths [40], where axial coercive fields almost vanish and magnetization processes become preponderantly reversible [41]. This decrease in the axial coercive field values for shorter ferromagnetic segments could explain the broadening of switching field distributions at higher lengths by the presence of shorter ferromagnetic segments.

## 6. Conclusion

In this paper we presented a theoretical model and an experimental approach to the identification of the interaction field in arrays of ferromagnetic barcode nanowires. These two strategies were applied in order to evaluate the interaction field in arrays containing barcode nanowires with three different magnetic loads and a very good agreement was obtained. The proposed methods can give an important insight into the morphology of the magnetic nanomaterials, since quantitative information about individual nano-objects may be extracted from macroscopic measurements of their arrays.

## References

- [1] Nielsch K, Wehrspohn R B, Barthel J, Kirschner J, Gosele U, Fischer S F and Kronmüller H 2001 *Appl. Phys. Lett.* **79** 1360
- [2] Darques M, Encinas A, Vila L and Piroux L 2004 *J. Phys.: Condens. Matter* **16** S2279
- [3] Barbic M 2002 *J. Magn. Magn. Mater.* **249** 357
- [4] Prina-Mello A, Diao Z and Coey J M D 2006 *J. Nanobiotechnol.* **4** 9
- [5] Tanase M, Bauer L A, Hultgren A, Silevitch D M, Sun L, Reich D H, Searson P C and Meyer G J 2001 *Nano Lett.* **1** 155
- [6] Reich D H, Tanase M, Hultgren A, Bauer L A, Chen C S and Meyer G J 2003 *J. Appl. Phys.* **93** 7275
- [7] Fan D L, Zhu F Q, Cammarata R C and Chien C L 2005 *Phys. Rev. Lett.* **94** 247208
- [8] Hangarter C M and Myung N V 2005 *Chem. Mater.* **17** 1320
- [9] Hangarter C M, Rheem Y, Yoo B, Yang E-H and Myung N V 2007 *Nanotechnology* **18** 205305
- [10] Wang A A, Lee J, Jenikova G, Mulchandani A, Myung N V and Chen W 2006 *Nanotechnology* **17** 3375
- [11] Zhao S, Clime L, Chan C, Normandin F, Roberge H, Yelon A, Cochrane R W and Veres T 2006 *J. Nanosci. Nanotechnol.* **7** 381
- [12] Cho J U, Wu J H, Min J H, Lee J H, Liu H-L and Kim Y K 2007 *J. Magn. Magn. Mater.* **310** 2420
- [13] Choi J-R, Jun S, Ju H and Cheon J 2005 *Nano Lett.* **5** 2179
- [14] Lee J H, Wu J H, Liu H L, Cho J U, Cho M K, An B H, Min J H, Noh S J and Kim Y K 2007 *Angew. Chem. Int. Edn* **46** 3663
- [15] Nicewarner-Pena S R, Freeman G, Reiss B D, He L, Pena D, Walton I D, Cromer R, Keating C D and Natan M J 2001 *Science* **294** 137
- [16] Clime L and Veres T 2007 *J. Magn. Magn. Mater.* **314** 11–5
- [17] Beleggia M, Tandon S, Zhu Y and De Graef M 2004 *J. Magn. Magn. Mater.* **278** 270
- [18] Strijkers G J, Dalderop J H J, Abroeksteeg M A, Swagten H J M and de Jonge J M 1999 *J. Appl. Phys.* **86** 5141
- [19] Rivas J, Kazadi Mukenga Bantu A, Zaragoza G, Blanco M C and López-Quintela M A 2002 *J. Magn. Magn. Mater.* **249** 220
- [20] Aign T *et al* 1998 *Phys. Rev. Lett.* **81** 5656
- [21] García J M, Asenjo A, Velázquez J, García D and Vázquez M 1999 *J. Appl. Phys.* **85** 5480
- [22] Prida V M, Pirota K, Navas D, Asenjo A, Hernández-Vélez M and Vázquez M 2007 *J. Nanosci. Nanotechnol.* **7** 272
- [23] Vázquez M, Hernández-Vélez M, Pirota K, Asenjo A, Navas D, Velázquez J, Vargas P and Ramos C 2004 *Eur. Phys. J. B* **40** 1434
- [24] Vázquez M *et al* 2004 *Physica B* **343** 395
- [25] Vázquez M, Pirota K, Hernández-Vélez M, Prida V M, Navas D, Sanz R, Batallan F and Velázquez J 2004 *J. Appl. Phys.* **95** 6642
- [26] Velázquez J, Pirota K and Vázquez M 2003 *IEEE Trans. Magn.* **39** 3049
- [27] Velázquez J and Vázquez M 2002 *IEEE Trans. Magn.* **38** 2477
- [28] Clime L, Béron F, Ciureanu P, Ciureanu P, Cochrane R W and Yelon A 2006 *J. Magn. Magn. Mater.* **299** 487
- [29] Clime L, Ciureanu P and Yelon A 2006 *J. Magn. Magn. Mater.* **297** 60
- [30] Clime L, Yelon A and Veres T 2007 *J. Appl. Phys.* **102** 013903
- [31] Masuda H and Fukuda K 1995 *Science* **9** 1466
- [32] Zhao S, Chan K, Yelon A and Veres T 2007 *Nanotechnology* **18** 245304
- [33] Herreros J, Barandiaran J M and Garcia-Arribas A 1996 *J. Non-Cryst. Solids* **201** 102
- [34] Della Torre E and Vajda F 1994 *IEEE Trans. Magn.* **30** 4987
- [35] Samwell E O, Bissell P R and Lodder J C 1993 *J. Appl. Phys.* **73** 1353
- [36] Della Torre E 1965 *IEEE Trans. Audio Electroacoust.* **14** 86
- [37] Stancu A, Stoleriu L and Cherchez M 2001 *J. Magn. Magn. Mater.* **225** 411
- [38] Hertel R 2002 *J. Magn. Magn. Mater.* **249** 251
- [39] Wernsdorfer W, Hasselbach K, Benoit A, Barbara B, Doudin B, Meier J, Ansermet J-P and Mailly D 1997 *Phys. Rev. B* **55** 11552
- [40] Sellmyer D J, Zheng M and Skomski R 2001 *J. Phys.: Condens. Matter* **13** R433
- [41] Kikuchi N, Okamoto S, Kitakami O, Shimada Y, Kim S G, Otani Y and Fukamichi K 2001 *IEEE Trans. Magn.* **37** 2082